Bakker A., Van den Akker H.E.A. (1994) Gas-Liquid Contacting with Axial Flow Impellers. Chemical Engineering Research and Design, TransIChemE Vol. 72, Number A4, July 1994, page 573-582.

GAS-LIQUID CONTACTING WITH AXIAL FLOW IMPELLERS

A. BAKKER and H. E. A. VAN DEN AKKER

Kramers Laboratorium voor Fysische Technologie, Delft University of Technology, Delft, The Netherlands

This paper focuses on the gas-dispersion characteristics of axial flow impellers. Various impellers are compared: an inclined blade impeller with flat blades, an A315 impeller and a Leeuwrik impeller. The goal is to gain insight in the gas-dispersion properties of such axial flow impellers. Therefore, the effects of impeller position and sparger geometry on flow pattern, power consumption and mass transfer are studied in a vessel 0.444 m in diameter, using liquids of different viscosity.

The power consumption is strongly related to the different flow patterns and different types of cavities. Under certain conditions time-dependent, asymmetrical flow patterns can occur. The sparger type influences both the power needed to prevent flooding and the overall mass transfer coefficient k_1a. The liquid viscosity does not affect the basic hydrodynamic phenomena in the vessel for viscosities not exceeding 80 mPa s.

Keywords: mixing; impeller; agitation; gas-liquid flow; mass transfer; gas holdup

INTRODUCTION

Stirred reactors are often used for dispersing gases into liquids. Although traditionally many of these gas-liquid reactors are equipped with simple impellers like the radial pumping disc turbine, the development of so-called hydrofoil impellers has led to an increased interest in the use of axial flow impellers. In general, the manufacturers claim that at a given power input such modern hydrofoil impellers are capable of dispersing more gas and of yielding higher mass-transfer coefficients than traditional impellers. As data in the open literature about these hydrofoil impellers are scarce, it is difficult to assess these claims.

This paper focuses on the gas-dispersion characteristics of axial flow impellers in general, and hydrofoil impellers in particular. Apart from a simple pitched blade turbine (PBT), the Leeuwrik impeller and the Lightnin A315 were tested. The goal was to gain insight in the gas-dispersion properties of profiled and non-profiled axial flow impellers by linking power consumption and mass transfer to the flow pattern and the impeller hydrodynamics. Hence, the relation between flow pattern power consumption and mass transfer has been studied in a vessel being 0.444 m in diameter using liquids of different viscosity and various sparger types.

LITERATURE

Because of the industrial importance of gas-liquid stirred vessels, their hydrodynamics has been the subject of extensive research[1] and several reviews on this subject can be found in the literature[2–4]. In particular, the hydrodynamic properties of the radially pumping disc turbine have been investigated thoroughly. This has led to a proposal for improving the design by curving the blades[5]. The disc turbine is very effective in dispersing gas by breaking up the gas bubbles, but it has a relatively low hydraulic efficiency, which results in a low 'flow per unit power'. Further disadvantages of the disc turbine are the high levels of the shear stress in the vicinity of the impeller, a non-uniform distribution of energy dissipation rate in the vessel[6] and a low gas-holdup in the lower part of the vessel[7,8].

Therefore, research is shifting towards the properties of axially pumping impellers which have a higher hydraulic efficiency and effect a more uniform distribution of energy dissipation rate in the vessel. These impellers further create lower levels of shear stress in the vicinity of the impeller. Axial flow impellers can be conveniently classified into two groups: simple impellers with flat inclined blades (pitched blade turbines), and so-called hydrofoil impellers with profiled blades. Although axial flow impellers can be used pumping upwards, in this project they will only be studied in the downwards pumping mode.

During the present research project an inclined blade impeller, an A315 impeller and the Leeuwrik impeller were tested. The Leeuwrik impeller is described by Bakker and Van den Akker[9] and Bakker[10].

The use of pitched blade turbines and disc turbines for two-phase and three-phase mixing has been extensively discussed by Chapman *et al.*[11,12]. These authors found that large torque fluctuations could occur when pitched blade turbines are used in the downwards pumping mode. Further, they compared the gas-handling characteristics and power consumption of various impeller types.

0263-8762/94/$05.00 + 0.00

Warmoeskerken *et al.*[13] gave a description of the hydrodynamic properties and of the process of cavity formation with pitched blade turbines. They distinguished two gas loading regimes: indirect loading and direct loading. Indirect loading occurs when the gas is pumped downwards and enters the impeller only upon recirculation. At high gassing rates, however, the downward liquid flow will not be sufficiently strong to overcome and deflect the rising gas flow; hence the gas will rise directly into the impeller. This situation is called direct loading. These authors also reported that the mass transfer efficiency of a downwards pumping pitched blade turbine, based on the power demand, is at least as good as that of disc turbines.

Information about hydrofoil impellers in the open literature is relatively scarce. Oldshue *et al.*[14] reported that the A315 is capable of dispersing 86% more air than a disc turbine at the same power input. In a water/air system mass transfer could be enhanced by 30% on the average by using an A315 system rather than a conventional disc turbine system. Later, Lally and Post[15] reported a much smaller difference between the A315 and the disc turbine. According to their results an improvement of $\pm 5\%$ in mass transfer rate can be achieved by using an A315 instead of a disc turbine.

IMPELLER DESIGN CONSIDERATIONS

The impeller in a gassed stirred vessel has to meet several requirements. The ideal impeller would both effect a strong liquid flow with homogeneously distributed turbulence levels, create a homogeneous gas dispersion, and in the meantime break up the gas bubbles to increase the interfacial area. Since no impeller will be capable of meeting all these requirements, two main design strategies can be followed.

The first strategy leads to the design of radially pumping impellers like the disc turbine and the concave blade turbine[5]. These impellers have a relatively low pumping efficiency and create extremely large shear stresses in the impeller region. As a result of their flow patterns, all the gas sparged into the vessel enters the impeller before being dispersed in small bubbles. Although the liquid velocities effected by the disc turbine are relatively low and the turbulence distribution is far from homogeneous, the small bubble size created by the impeller leads to small bubble slip velocities. As a consequence, the bubbles follow the main liquid flow relatively well, and significant levels of gas recirculation can be reached.

The second strategy is to try to increase the homogeneity of the gas dispersion and the mixing by increasing the liquid velocities and the turbulence levels in the liquid bulk. This can be done by designing an impeller with a high pumping efficiency. The pumping efficiency can be optimized by designing impellers with narrow profiled blades, like an air-wing.

Unfortunately, one of the problems with the use of such axially pumping impellers is that due to early cavity formation, the pumping capacity will decrease with increasing gassing rate. Thus, for such impellers to be able to operate, the sensitivity for gassing has to be decreased. This can be done by increasing the so-called solidity ratio of the impeller, as with the Lightnin A315 impeller.

The solidity ratio SR[16] is defined as the total blade area $n_b A_b(!)$ divided by the area of the circle that encloses the projection in axial direction of the impeller onto a plane:

$$SR = \frac{n_b A_b}{\frac{\pi}{4} D^2} \tag{1}$$

An impeller with a high solidity ratio is capable of operating at a high pressure loading, which is advantageous in gas-liquid systems and equally in high viscosity fluids.

The advantage of a high solidity ratio can be described in more detail by looking at the thrust F_T delivered by the impeller. The thrust F_T induces a mean circulatory flow through the vessel, the strength of which strongly depends on the flow resistance. This resistance results from the vessel geometry (D/T ratio, bottom profile, impeller-bottom clearance, baffle design, etc.). Therefore, the impeller has to overcome a pressure difference $\langle \Delta p_f \rangle$, which is proportional to the velocity head of the circulatory flow:

$$\langle \Delta p_f \rangle = K_w \tfrac{1}{2} \rho \langle v_{ax} \rangle^2 \tag{2}$$

To maintain this pressure difference the impeller must deliver a thrust F_T:

$$F_T = \frac{\pi}{4} (D^2 - d_{hub}^2) \langle \Delta p_f \rangle \tag{3}$$

In addition, the thrust F_T is proportional to the thrust loading, $\langle \Delta p_b \rangle$, being the average pressure increase over the impeller blades from suction side to pressure side. Hence:

$$F_T = n_b A_{b,\perp} \langle \Delta p_b \rangle \tag{4}$$

Here $A_{b,\perp}$ denotes the projected area of one blade. Combining equations (2), (3) and (4) results in:

$$\langle \Delta p_b \rangle = \frac{F_T}{n_b A_{b,\perp}} = K_w \tfrac{1}{2} \rho \langle v_{ax} \rangle^2 \frac{\frac{\pi}{4}(D^2 - d_{hub}^2)}{n_b A_{b,\perp}} \tag{5}$$

It is necessary to keep $\langle \Delta p_b \rangle$ as low as possible for two reasons. The first reason is that at a low $\langle \Delta p_b \rangle$ stalling will occur less easily. Stalling is the loss of pumping capacity due to separation of the boundary layer at the suction side of the impeller blade. The second reason is that due to the lower pressure at the suction side of the impeller blade, gas will accumulate there and this will eventually lead to the formation of large gas filled cavities and consequently to loss of pumping capacity. In the case of a low $\langle \Delta p_b \rangle$ this will occur less easily and the impeller pumping capacity will be less dependent on the gassing rate. It will therefore be clear from Equation (5) that a high projected blade area ratio $R_{b,\perp}$

$$R_{b,\perp} = \frac{n_b A_{b,\perp}}{\frac{\pi}{4}(D^2 - d_{hub}^2)} \tag{6}$$

Table 1. Solidity ratio, blade area ratio and other variables.

Impeller	SR	$R_{b,\perp}$	n_b	D(m)	Po	Fl_1
A315	90%	77%	4	0.178	0.76	0.74
Leeuwrik	160%	80%	6	0.168	2.55	—
PBT	60%	45%	6	0.176	1.55	0.81

will increase the performance of the system. This roughly corresponds with increasing the solidity ratio. The advantage of a large $R_{b,\perp}$ is confirmed by the fact that it has repeatedly been found that pitched blade turbines in gassed systems perform better when the number of blades is increased. Frijlink *et al.*[17] for example, found that six blade inclined blade turbines performed better with respect to suspending solids in gassed systems than four blade impellers.

Note that the projected blade area ratio is not the only parameter affecting cavity formation and stalling and that these processes will also depend on the shape of the impeller blades.

The values for the solidity ratio, $R_{b,\perp}$ and the number of blades are listed in Table 1, together with the impeller power number:

$$Po = \frac{P}{\rho N^3 D^5} \tag{7}$$

and the impeller pumping number:

$$Fl_1 = \frac{Q_1}{ND^3} \tag{8}$$

Here P is the power consumption of the impeller and Q_1 is the liquid flow rate through the impeller. It can be seen that the Leeuwrik impeller has the largest solidity ratio, but that the A315 has the largest blade area ratio. The impeller pumping number is calculated from LDV data[18]. No correlation between SR or $R_{b,\perp}$ and Po or Fl_1 is found.

EXPERIMENTAL SET-UP

A flat-bottomed plexiglass vessel of diameter T= 0.444 m was used in all experiments. The vessel was equipped with four baffles (width $W = 0.077\ T$, mounted at a distance $0.023\ T$ from the wall). The liquid height H was equal to the tank diameter T. Experiments were done with distilled water and glycerol solutions of viscosities $\eta = 36$ mPa s ($\rho = 1190$ kg m^{-3}) and $\eta =$ 80 mPa s ($\rho = 1220$ kg m^{-3}). The diameter of the impellers was $D = 0.4\ T$. The impellers were placed either at a distance $C = 0.75\ D$ or a distance $C = D$ from the vessel bottom. The blade width for the pitched blade turbine was $W_b = 0.2\ D$.

The power demand was calculated from the impeller rotational speed and the torque exerted by the impeller. The torque was determined with a Vibro-torque transducer mounted in the shaft. The overall gas-holdup could be determined with an ultrasonic liquid level meter.

Several spargers were tested: a pipe sparger (PS), a small ring sparger (SRS, $d_s = 0.4\ D$), a large ring sparger (LRS, $d_s = 0.75\ D$) and a quadruple pipe sparger (QPS). The QPS was configured to the design of Weetman[19]

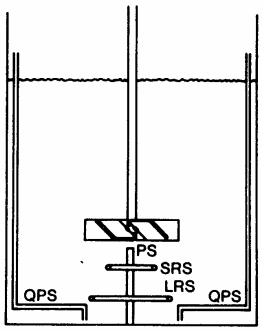

Figure 1. The four investigated sparger types: a pipe sparger (PS), a small ring sparger (SRS), a large ring sparger (LRS) and a quadruple pipe sparger (QPS).

and consists of four inlet tubes, pointing down at the vessel bottom. The distance between the ring spargers and the impeller could be varied. A schematic view of the spargers and the vessel is shown in Figure 1.

The mass transfer coefficient $k_l a$ was determined using a dynamic measurement method, assuming perfect mixing in the gas-phase[10]. The experiments were performed in distilled water. The superficial gas velocity was $v_{sg} = 0.01$ m/s. The mass transfer experiments reported in this paper were performed with the impeller mounted at a clearance $C/D = 0.75$.

HYDRODYNAMICS

The Gassed Flow Pattern and Impeller Hydrodynamics

In this section, the experiments performed with water will be reported first and later the influence of an increase in viscosity will be discussed.

The gassed flow pattern as a function of impeller speed and of gassing rate was studied visually. Further, the process of cavity formation was photographed. This was done for all three impellers investigated. It turned out that the characteristics of the pitched blade turbine and the A315 impeller are very similar.

The results for the A315 are illustrated in Figure 2. At low gassing rates and/or high impeller speeds, the gassed flow pattern is symmetrical. Gas reaches the impeller only due to recirculation (indirect loading) and vortex cavities are formed (Figure 2A). If the impeller speed is decreased, or the gassing rate increased, the gas is still pumped downwards (indirect loading) but the impeller is not capable of recirculating all the gas anymore, the gas escapes from the vessel on one side in a large gas cloud while on the other side the gas is recirculated in a small loop. As a result, the flow pattern is asymmetrical and the gas cloud can be seen precessing through the vessel with a period between approximately 1 and 30 minutes, depending on exact sparger geometry, gassing rate and impeller speed. In this situation growing cavities are formed (Figure 2B).

At still higher gassing rates the impeller is not capable of deflecting the rising gas flow and gas rises into the impeller directly (direct loading). In this situation large

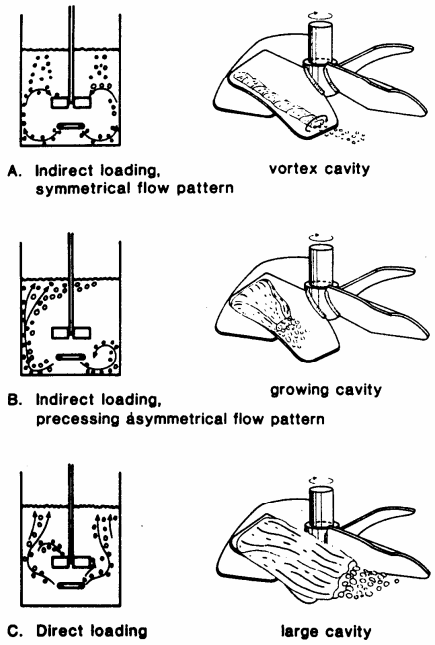

Figure 2. The cavity formation process and the flow regimes for the A315.

cavities are formed (Figure 2C) and the flow pattern is dominated by the rising gas flow rather than by the impeller. This situation can also be called flooding. The transitions between the flow patterns are not sharp and often give rise to oscillations. In particular, the indirect loading to direct loading transition was found to result in large torque fluctuations. This has already been observed for pitched blade turbines by Chapman *et al.*[11].

In general, the different flow patterns and hydrodynamic regimes of the A315 and the inclined blade impeller are very alike. The asymmetrical flow pattern was also found with the inclined blade impeller. This has not been reported before in the literature. The clinging cavities which are formed with the inclined blade impeller[13] were not observed with the A315. This may be an indication that the vortices formed at the blade edges are stronger with the PBT than with the A315.

The Asymmetrical Flow Pattern

The precessing asymmetrical flow pattern depicted in Figure 2B is quite interesting. Such asymmetries were already observed for other hydrofoil impellers[20] and can also be seen with pitched blade turbines. Further, these time dependent asymmetries have been observed on an industrial scale in the gold cyanidation process[21]. This suggests that these asymmetries are inherent to a lot of systems equipped with single axial flow impellers.

The asymmetrical flow pattern consists of a gas cloud rising up on one side of the vessel, and a short gas circulation loop on the other side of the vessel. Further, different types of vortices can be observed (Figure 3). The gas cloud is either stable, and stays on one side of

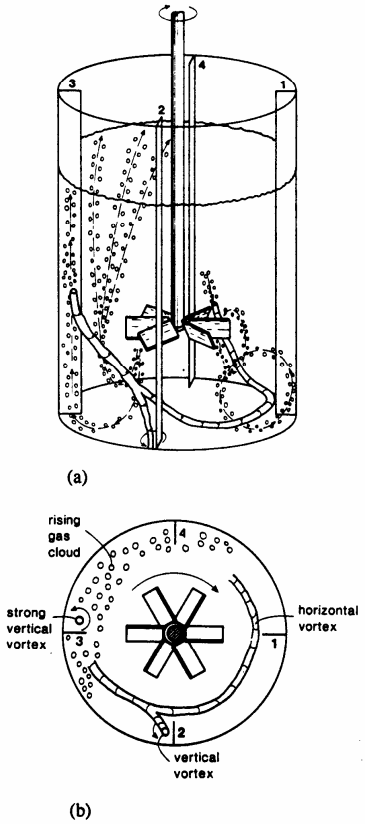

Figure 3. The vortex system and the precessing asymmetrical flow pattern.

the vessel, or it precesses slowly around the vessel. For the PBT, the direction of precession was always equal to the direction of rotation of the impeller. In contrast, for the A315 the direction of precession was often opposite to the direction of rotation of the impeller.

The mechanism behind the precessing motion is still unclear, especially for those cases where the direction of precession is opposite to the direction of rotation of the impeller. Bakker and Van den Akker[22] suggested a mechanism for those cases where the impeller rotational direction and the precessing direction are the same.

This mechanism can be described in detail with the help of the sketch in Figure 3. It is essential to understand that in a vessel equipped with an axial flow impeller two opposite kinds of vortex motion are interacting. The impeller induces both a tangential flow and an axial flow. Due to the tangential flow, vertical vortices are formed behind the baffles. On the other hand, the axial flow generates horizontal vortices lying near to the vessel bottom. The interaction between these horizontal and vertical vortices may lead to instabilities and an asymmetrical flow condition, depending on the ratio of the strength of the main, axial flow and the strength of the secondary, tangential flow.

At low gassing rates the impeller acts as an efficient pump and the flow pattern in the vessel is dominated by

the axial flow, and the associated circulation loops with the horizontal vortex in the centre. Under these conditions instabilities may not get the opportunity to grow. At increasing gassing rate the pumping efficiency of the impeller decreases due to cavity formation: the strength of the axial flow induced by the impeller decreases faster than the strength of the tangential flow. At the same time, the momentum of the gas entering the vessel increases. The rising gas flow disturbs the recirculation loops and promotes and strengthens the long vertical vortices induced by the tangential flow. The combination of these effects lead to the asymmetrical flow pattern depicted in Figure 3.

In this case the horizontal vortex caused by the axial flow lies near the bottom in front of baffle 1. Behind baffle 2 a vertical vortex is formed which bends sideways and joins with the horizontal vortex. Due to both the rising gas flow and the tangential flow caused by the impeller, a strong vertical vortex is created behind baffle 3. The gas leaves the vessel in a cloud which roughly lies between baffle 3 and 4. There is no tangential vortex to be seen behind baffle 4 since the direction of rotation of this would-be vortex is opposed by the horizontal vortex in front of the baffle 1. Due to the tangential motion induced by the impeller, the diagonal vortex between baffle 2 and 3 is gradually bending more horizontal, towards baffle 3. At the same time, the gas cloud from baffle 3 to 4 shifts gradually in the direction of baffle 4 to baffle 1 and the vertical vortex behind baffle 3 also bends gradually in the direction of baffle 4. Due to the fact that now a small vertical vortex behind baffle 4 is formed since more gas is rising up there, the horizontal vortex in front of baffle 1 moves towards baffle 2, and joins with the vertical vortex behind baffle 3. As a consequence, the whole flow pattern, including the rising gas cloud and the horizontal/vertical vortex system, slowly precesses in the direction of rotation of the impeller.

The period of precession depends on gassing rate, impeller speed, power consumption and sparger position. Typical values range from one minute to thirty minutes. To investigate these phenomena further, the local gas holdup at $2r/T = 0.7$ and $z/H = 0.6$ has been measured with an optical fibre probe (Bakker, 1992) in the plane midway between the baffles. A typical gas holdup signal is shown in Figure 4. It can be seen that there is a strong fluctuation in the local gas holdup as a result of the periodicity in the flow pattern. The precessing frequency

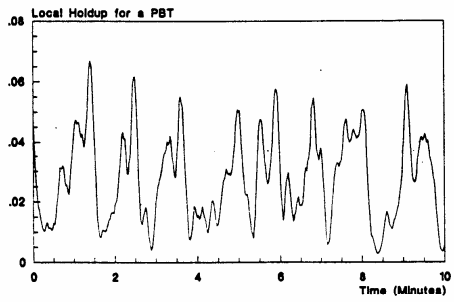

Figure 4. Time dependent local gas holdup with the pitched blade turbine (N = 5 Hz, $v_{sg} = 0.0067$ m/s, $2r/T = 0.7$, $z/H = 0.6$).

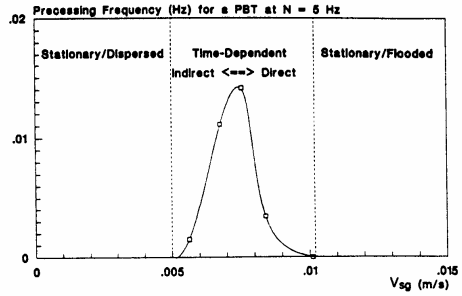

Figure 5. Precessing frequency of the gas cloud for the pitched blade turbine as a function of superficial gas velocity.

has been calculated from the holdup signals with the aid of Fast Fourier Transforms. Figure 5 shows the precessing frequency of the gas cloud for a pitched blade turbine (PBT) as a function of superficial gas velocity at a constant impeller speed. It can be seen that three regimes can be distinguished, steady-state and dispersed, low frequency time-dependent, and steady state and flooded. The highest precessing frequency is found near the indirect loading to direct loading transition.

These are preliminary results and a lot of questions regarding these time-dependent flow patterns remain to be answered. Therefore these phenomena will be the subject of further study.

The Link with Power Consumption

The effect of gassing on power consumption is the direct result of changes in the impeller hydrodynamics and the flow patterns as discussed above, and can be illustrated by the P_g/P_u vs. Fl_g curves for different impeller speeds.

Figure 6 shows the P_g/P_u curves at constant impeller speeds for the PBT. With the PBT the power consumption shows a steep decrease, which was visually found to be related to transition from indirect to direct loading, at a gas flow number Fl_g between 0.02 and 0.04, depending on impeller speed.

Figure 7 shows the P_g/P_u curve at a constant impeller speed of $N = 5\ s^{-1}$ for the A315. The different regions in this curve correspond with the three different flow patterns and the different types of cavities described before (see also Figure 2). As with the PBT, the formation of large cavities at the indirect/direct loading transition

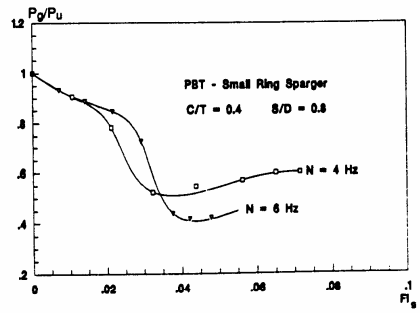

Figure 6. Power curves for the PBT at constant impeller speed.

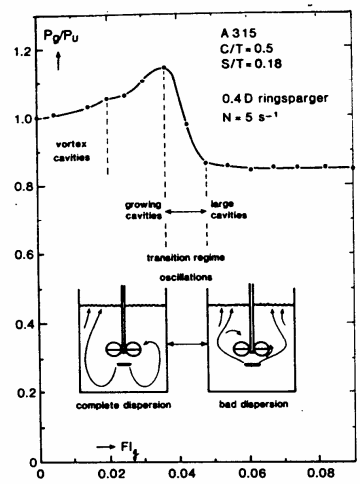

Figure 7. The relation between the gassed power consumption, the gassed flow pattern and the cavity formation process.

corresponds with a strong drop in power consumption (see also Figure 8).

The curves of the gassed power number Po_g vs. gas flow number Fl_g at a constant superficial gas velocity look quite different. Figure 9 shows the gassed power at three different superficial gas velocities for the PBT with a large ring sparger. When at a certain gassing rate the impeller speed is increased, starting from a low speed (high Fl_g), Po_g decreases until a minimum is reached,

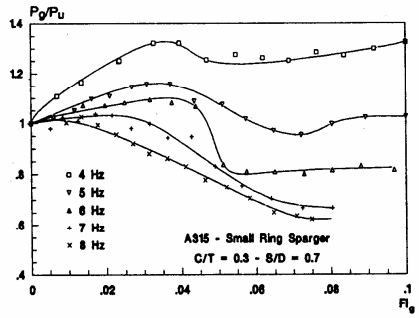

Figure 8. Power curves for the A315 at constant impeller speed.

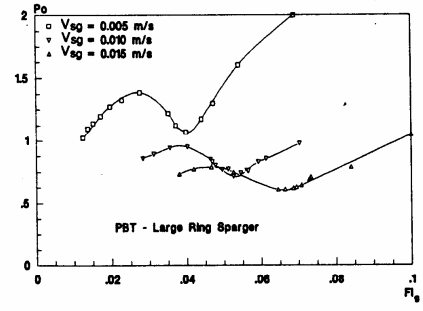

Figure 9. Power curves for the PBT at constant superficial gas velocity.

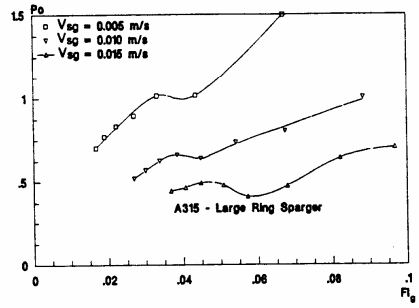

Figure 10. Power curves for the A315 at constant superficial gas velocity (large ring sparger).

probably due to an increase in cavity size. This minimum corresponds with the indirect/direct loading transition. After the large cavities have disappeared at this critical flow number $Fl_{g,c}$, corresponding with a critical specific power consumption $\langle \varepsilon_c \rangle = P_c/V_l$, the power number increases at increasing impeller speed until a maximum is reached. When the impeller speed is increased even further Po_g decreases again due to an increase in gas recirculation. The power curves for the A315 (Figure 10) are similar to those of the PBT although the transitions are less pronounced.

In general it can be concluded that the gassed power consumption depends both on the impeller type and sparger configuration, due to differences in the induced flow patterns and cavity structures.

Influence of Impeller Type

The impellers are compared on basis of the minimum power consumption necessary for full gas dispersion $\langle \varepsilon_c \rangle = P_c/V_l$.

Figure 11 shows $\langle \varepsilon_c \rangle$ for all three impellers compared as a function of v_{sg}. It can be seen that the Leeuwrik impeller has the worst performance. At $v_{sg} = 0.005$ m/s the difference between the PBT and the A315 is small, but at higher gassing rates the A315 gives a better performance. This may be due to the fact that the A315 is capable of maintaining a stronger liquid flow at high gassing rates than the pitched blade turbine.

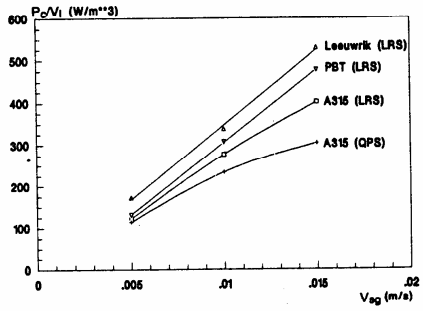

Figure 11. The minimum power consumption necessary to prevent direct loading.

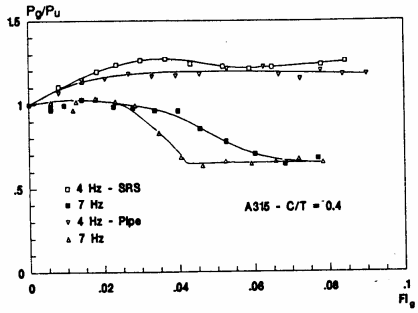

Figure 12. Power curves for the A315 with a small ring sparger and a pipe sparger at constant impeller speed.

The Effect of Sparger Configuration

The performance of various spargers has been tested with the A315 and the PBT with water. Since the results were very similar, the main conclusions will be illustrated with the A315 data only. Figure 12 shows a comparison between the power curves for the small ring sparger (SRS) and the pipe sparger (PS). It is clear that the power drop in the curves occurs earlier for the pipe sparger than for the ring sparger. This means that with the ring sparger less power is needed for dispersing a certain amount of gas.

Figure 13 shows the effect of impeller to sparger separation distance S. When this distance is increased the power drop takes place at a higher gassing rate. Again this means that with respect to the power needed to disperse a certain amount of gas a large separation distance is beneficial.

The minimum power consumption $\langle \varepsilon_c \rangle$ necessary for preventing the impeller from flooding has been determined as a function of gassing rate for the quadruple pipe sparger (QPS) and the large ring sparger mounted at $S = 0.6\ D$ (Figure 11). It is clear that at low gassing rates there is hardly any difference between these two sparger configurations but that at high superficial gas velocities the QPS performs better than the LRS.

In general it can be concluded that less power is needed to prevent the impeller from flooding when the gas input is moved outward or further away from the impeller (Figure 1). This may be attributed to two effects. First,

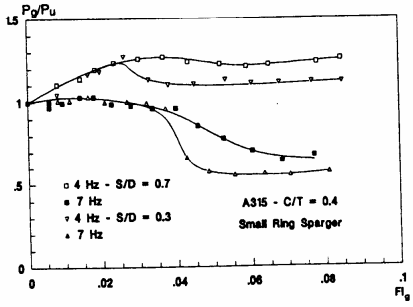

Figure 13. Power curves for the A315, small ring, sparger, two impeller to sparger separation distances, constant impeller speed.

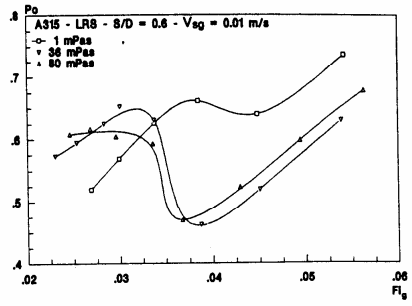

Figure 14. Power curves for the A315 at three liquid viscosities.

moving the sparger outward and/or downwards will lead to a lower gas holdup below the impeller, and to a lower overall gas holdup. This results in a lower static pressure difference which has to be overcome by the impeller; as a consequence flooding will occur less easily. The second effect is related to the momentum of the input gas. The rising gas will induce an upward fluid motion, which opposes the downward flow below the impeller. The momentum of the input gas has less effect when the gas is supplied in the high velocity region close to the vessel bottom.

Influence of Liquid Viscosity

The Po_g vs. Fl_g curves were measured for different liquid viscosities, for the A315 impeller with the LRS mounted at an impeller to sparger separation distance $S = 0.6\ D$ (Figure 14). Although there are quantitative differences with respect to the positions of the minima and maxima, the basic shape of the curves is the same for all viscosities.

The power curves for the PBT at 80 mPa s are also very similar to those measured for distilled water (Figure 15). Hence it can be concluded that the hydrodynamic processes in the vessel are the same for liquid viscosities within the investigated range from $\eta = 1$ mPa s to $\eta = 80$ mPa s.

It is interesting to see that for the A315 the critical power consumption $\langle \varepsilon_c \rangle = P_c/V_l$ increases almost linearly with liquid viscosity within the investigated range (Figure 16).

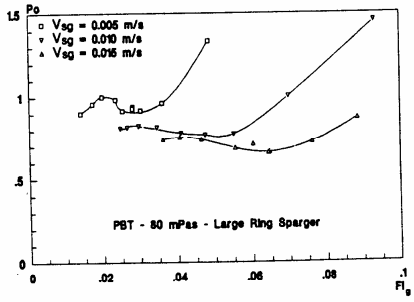

Figure 15. Power curves for the PBT at 80 mPa s.

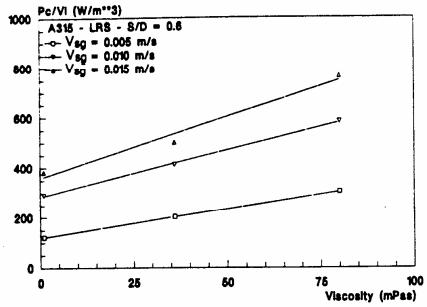

Figure 16. Minimum power consumption to prevent direct loading vs. viscosity, A315.

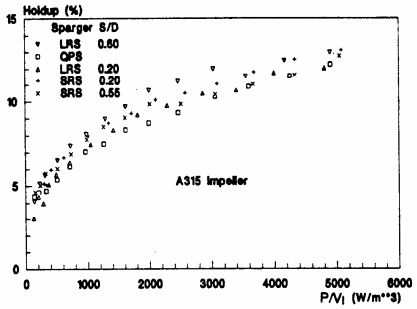

Figure 18. Influence of sparger configuration on holdup (A315, $v_{sg} = 0.01$ m/s).

MASS TRANSFER AND GAS-HOLDUP

The quadruple pipe sparger (QPS), the large ring sparger (LRS) placed at S = 0.6 D and the small ring sparger (SRS) at S = 0.5 D were also compared with respect to mass transfer performance (Figure 17). It can be seen from Figure 17 that all data points for the SRS are above all data points for the LRS, which are all lying above the data points for the QPS. This means that there is a significant influence of sparger type on the mass transfer coefficient.

On the other hand the influence of sparger type on gas holdup is not as clear. For the PBT no significant influence of the sparger type on gas holdup was found. For the A315 (Figure 18) the holdup curves for the different sparger types tend to separate for power consumptions between 1000 and 4000 W/m^{-3} but without any clear order.

The diffuse effects of sparger type on the overall gas holdup might be due to the fact that there are several opposed mechanisms interacting. When the sparger is mounted close to the impeller, this will lead to a high gas holdup below the impeller. This will, however, affect the static pressure difference which has to be overcome by the impeller. As a result the impeller pumping capacity may decrease, which will lead to a reduced recirculation rate. Further, the high holdup in the turbulent region below the impeller will, in water, lead to an increase in the coalescence rate and consequently to larger bubbles. Since large bubbles have larger rise velocities, they will escape from the vessel faster, which again leads to lower gas holdup.

Further, there are effects of a secondary flow loop below the pitched blade turbine[17,18]. The position of the sparger with respect to this secondary recirculation loop will also affect the gas holdup below the impeller. How the overall gas holdup is affected by the sparger type and position will depend on the exact geometry, impeller type, impeller speed and gassing rate.

This suggests that the influence of sparger type on k_la may not fully be attributed to a difference in overall gas holdup, but is merely due to the distribution of the gas in the vessel. The mass transfer rate will not only depend on the gas holdup and bubble size but also on the value of k_l. Since the turbulence distribution will be non-homogeneous, significant differences in k_l throughout the vessel can be expected. Concentrating the gas in the outflow of the impeller, where turbulence levels and k_l are large will lead to an increase in k_la. To be able to give a more detailed explanation of how geometrical changes affect k_la, it will be necessary to analyse the local distributions of the gas holdup, bubble size and turbulence intensity.

It was found that with respect to the minimum power consumption necessary to disperse the gas and the stability of the system, it is advantageous to use a large sparger mounted far away from the impeller. It has now become clear that it will depend on what should be optimized, stability of operation or mass transfer performance, which sparger type should be chosen.

In Figure 19 the four impellers are compared on basis

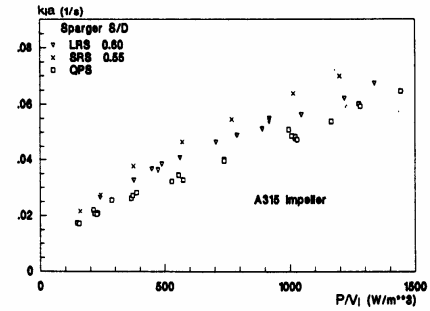

Figure 17. Influence of sparger configuration on k_la (A315, $v_{sg} = 0.01$ m/s).

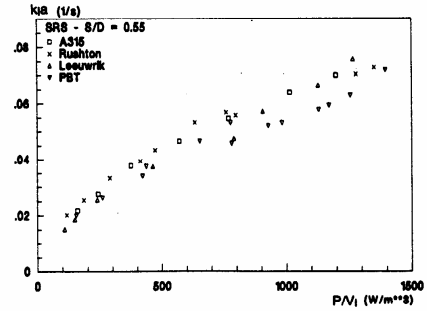

Figure 19. Mass transfer coefficient for various impellers ($v_{sg} = 0.01$ m/s).

of overall k_la. It turns out that the difference between the A315, the Leeuwrik impeller and the DT is small but that the PBT has the worst performance of the impellers investigated. The fact that there are only small differences between the A315, the Leeuwrik impeller and the DT may be an indication that both the gas dispersion strategies described above may work. Both creating very small bubbles, but a relatively weak liquid flow (disc turbine) and creating a relatively strong liquid flow but with only little bubble break-up by the impeller (A315) can lead to high mass transfer coefficients. The fact that the PBT has the worst performance is probably caused by its relatively low pumping efficiency under gassed conditions, when compared with the A315.

CONCLUSIONS

The hydrodynamic properties of three axial flow impellers have been investigated. Different flow patterns and different types of cavities were found and were shown to be strongly related to the power consumption.

The flow patterns found for the PBT and the A315 were very similar. At low gassing rates the gas is well dispersed and stable. The gas enters the impeller only after it is recirculated (indirect loading). When the gassing rate is increased, the gas will still be dispersed, but the system becomes unstable and slowly precessing asymmetrical flow patterns are found. The frequency of precession is dependent on the gassing rate, the impeller speed and the sparger geometry. A mechanism based on the interaction between horizontal and vertical vorticity is suggested for this time dependent behaviour. When the gassing rate is increased further the gas will enter the impeller directly (direct loading) before it is dispersed, and only little gas recirculation occurs.

The influence of the liquid viscosity on the hydrodynamics has been investigated for viscosities ranging from $\eta = 1$ mPa s to $\eta = 80$ mPa s. Within this range no qualitative changes in the basic flow patterns and the hydrodynamic regimes of the impellers were observed. The minimum power consumption to prevent the impeller from flooding, however, showed an almost linear increase with liquid viscosity.

The advantage of a large solidity ratio has been explained in detail in terms of the average pressure difference over the impeller blades. Although blade shape is also important, generally speaking an impeller with a large solidity ratio will be less susceptible to a decrease in pumping capacity when cavities are formed.

Different sparger types have been compared. It turns out that less power is needed to disperse the gas when the gas inlet is moved outward and/or closer to the vessel bottom. Those sparger configurations which are most effective in dispersing the gas, however, were found to yield a lower overall gas holdup and a lower mass transfer coefficient k_la than other sparger configurations. This is probably due to changes in the gas distribution and turbulence distribution throughout the vessel. In general, a 0.75 D ring sparger mounted at a separation distance $S = 0.6\,D$ will be a good compromise between gas handling capacities and mass transfer performance.

Of the three axial flow impellers investigated, the A315 has the best overall performance. The differences in k_la between the disc turbine, the A315 and the Leeuwrik impeller are negligible in those regimes where all the impellers are capable of dispersing the gas. The PBT yields a lower gas holdup and k_la than the other impellers.

The analysis of the gas-liquid hydrodynamics of stirred mixing vessels presented in this paper has led to several new insights. However, it has also become clear that the methods employed in this paper have their limits. Although they are very useful for classifying flow patterns and hydrodynamic regimes and for impeller comparison, it is very difficult to increase the fundamental understanding of the processes occurring inside the stirred gas-liquid dispersion, thus new methods have to be developed. It is expected that the application of experimental methods which allow the measurement of local properties of the gas-liquid dispersion, in combination with Computational Fluid Dynamics (CFD) and the development of appropriate models for the gas-liquid flow can overcome these problems. This will be the subject of further research.

NOMENCLATURE

A_b	area of one impeller blade
$A_{b,\perp}$	projected area of one impeller blade
C	impeller to bottom clearance
d_{hub}	impeller hub diameter
d_s	sparger diameter
D	impeller swept diameter
F_T	axial force exerted by the impeller (thrust)
Fl_l	impeller pumping number
Fl_g	gas flow number
H	liquid height
k_l	liquid side mass transfer coefficient
k_la	overall volumetric mass transfer coefficient
K_w	friction coefficient
n_b	number of impeller blades
N	impeller rotational speed
$\langle \Delta p_f \rangle$	average pressure increase at impeller
$\langle \Delta p_b \rangle$	the average pressure difference between the two sides of an impeller blade
P	power consumption
Po	impeller power number
Q_g	gassing rate
Q_l	liquid flow rate
$R_{b,\perp}$	projected blade area ratio
S	impeller-sparger separation
SR	solidity ratio
T	vessel diameter
v_{sg}	superficial gas velocity
$\langle v_{ax} \rangle$	average axial liquid velocity out of the impeller plane
W	baffle width
W_b	width of impeller blade

Greek Symbols

α	gas holdup
$\langle \varepsilon \rangle$	average energy dissipation rate density
ρ	density

Subscripts

c	critical, at the indirect/direct loading transition
g	gas, under gassed conditions or referring to gas phase
l	referring to liquid phase
u	ungassed conditions

Abbreviations

DT	Disc Turbine (Rushton Turbine)
LRS	Large ring sparger
LDV	Laser Doppler Velocimetry

PBT	Downwards pumping Pitched Blade Turbine, 6 blades at 45° blade angle
PS	Pipe sparger
QPS	Quadruple pipe sparger
SRS	Small ring sparger

REFERENCES

1. Nienow, A. W., 1990, Gas-dispersion performance in fermenter operation *Chem Eng Prog*, 2: 61–71.
2. Smith, J. M., 1985, Dispersion of gases in liquids *Mixing of Liquids by Mechanical Agitation*, Eds Ulbrecht J. J. and Patterson G. K., (Gordon and Breach Science Publishers).
3. Joshi, J. B., Pandit, A. B., Sharma, M. M., 1982, Mechanically agitated gas-liquid reactors *Chem Eng Sci*, 37: 813–844.
4. Nienow, A. W., Konno, M. and Bujalski, W., 1986, Studies on three-phase mixing: A review and recent results *Chem Eng Res Des*, 64: 35–42.
5. Warmoeskerken, M. M. C. G. and Smith, J. M., 1989, The hollow blade agitator for dispersion and mass transfer *Chem Eng Res Des*, 67: 193–198.
6. Laufhütte H. D. and Mersmann, A. B., 1985, Dissipation of power in stirred vessels *Proceedings 5th Eur Conf Mixing, Wurzburg, Germany, June 10–12*, 331–340.
7. Mann, R. and Hackett, L. A., 1988, Fundamentals of gas-liquid mixing in a stirred vessel: An analysis using networks of zones *Proceedings 6th Eur Conf Mixing, Pavia, Italy, May 24–26*, 321–328.
8. Weetman, R. J., 1989, Mixing apparatus European Patent Application 89109743.8.
9. Bakker, A. and Van den Akker, H. E. A., 1990, The use of profiled axial flow impellers in gas-liquid reactors, *Proc Fluid Mixing IV, Bradford, UK, September 11–13 1990 IChemE Symposium Series No 121*, 153–166.
10. Bakker, A., 1992, Hydrodynamics of stirred gas-liquid dispersions *PhD Thesis*, (Delft University of Technology, The Netherlands).
11. Chapman, C. M., Nienow, A. W., Cooke, M. and Middleton, J. C., 1983a, Particle-gas-liquid mixing in stirred vessels; Part 2: Gas-liquid mixing *Chem Eng Res Des*, 61: 82–95.
12. Chapman, C. M., Nienow, A. W., Cooke, M. and Middleton, J. C., 1983b, Particle-gas-liquid mixing in stirred vessels; Part 4: Mass Transfer and Final Conclusions *Chem Eng Res Des*, 61: 182–185.
13. Warmoeskerken, M. M. C. G., Speur, J. and Smith, J. M., 1984, Gas-liquid dispersion with pitched-blade turbines *Chem Eng Comm*, 25: 11–29.
14. Oldshue, J. Y., Post, T. A., Weetman, R. J. and Coyle, C. K., 1988, Comparison of mass transfer characteristics of radial and axial flow impellers *Proceedings 6th Eur Conf Mixing, Pavia, Italy, May 22–24*, 345–350.
15. Lally, K. S. and Post, T. A., 1991, Axial flow mixing impeller improves bioreactor performance, *MIXING XIII, Banff, Canada. June 10–15*, (Unpublished) (Engineering Foundation).
16. Oldshue, J. Y., 1989, Fluid mixing in 1989 *Chem Eng Prog*, 5: 33–42.
17. Frijlink, J. J., Bakker, A. and Smith, J. M., 1990, Suspension of solid particles with gassed impellers *Chem Eng Sci* 45: 1703–1718.
18. Bakker, A. and Van den Akker, H. E. A., 1994, Single phase flow in stirred reactors Trans IChem E, Part A. 72: 583–593.
19. Weetman, R. J., 1989, Mass-transfer mixing system especially for gas-dispersion in liquids or liquid suspensions US-Patent 4882098.
20. McFarlane, C., 1989, Power characteristics and gas-liquid hydrodynamics of the prochem maxflo-hydrofoil impeller *MIXING XII, Potosi, Missouri, USA* (Unpublished) (Engineering Foundation).
21. Koen, C., 1990, *Personal communication.*
22. Bakker, A. and Van den Akker, H. E. A., 1990, Gas liquid contacting with the Lightnin A315 impeller, effects of flow pattern AIChE Annual Meeting, Chicago, November 11–16, Session on Industrial Mixing and Scale-Up (Unpublished).

ACKNOWLEDGEMENT

These investigations were financially supported by the Netherlands Technology Foundation (STW, project DTN 40.0566). We are indebted to Lightnin for making available an A315 impeller.

ADDRESS

Correspondence concerning this paper should be addressed to Dr A. Bakker, Chemineer Inc, 5870 Poe Avenue, Dayton, OH 45414, USA.

The manuscript was communicated via our International Editor for Continental Europe, Dr A. D. Barber. It was received 29 October 1991 and accepted for publication after revision 17 August 1993.